The International Journal of Advanced Manufacturing Technology (2020) 108:1827–1838
https://doi.org/10.1007/s00170-020-05451-2

ORIGINAL ARTICLE

A new process chain combining cross-wedge rolling and isothermal forging for the forming of titanium alloy turbine blades

Junling Li[1] · Baoyu Wang[1] · Shuang Fang[2] · Ping Chen[1]

Received: 25 December 2019 / Accepted: 12 May 2020 / Published online: 2 June 2020
© Springer-Verlag London Ltd., part of Springer Nature 2020

Abstract
Titanium alloy blades are significantly important parts for aero-engine, and their special outline and production status requires an efficient and low-cost production process. In this paper, a new sequence for forming the titanium alloy blade using cross-wedge rolling (CWR) and isothermal forging was proposed. A finite element (FE) numerical model which contains the entire sequence, including the transfer process, CWR process, and isothermal forging process, was developed. And the axial displacement, strain-stress state, and temperature variation were analyzed based on its material properties of titanium alloy. The results showed that the billet experiences a smooth flowing in the center along the axial direction, and no large concavity occurs due to the higher viscosity. Moreover, the chilling effect of the dies was effectively counterbalanced by the deformation-heat near the surface, and there is no larger temperature difference. During the isothermal forging, the flash is symmetrically distributed around the fully filled blade and no obvious forming defects occur. Moreover, the novel sequence contributes to improving the deformed microstructure by accelerating the globularization of the long-strip alpha phase and increasing the volume fraction of the primary alpha phase. The technical feasibility of the novel sequence was verified by the corresponding experiments.

Keywords Titanium alloy · Blade · Cross-wedge rolling · Isothermal forging · Microstructure

1 Introduction

Significantly and urgently, it has become a bottleneck to design and manufacture aero-engines with a heavy-weight ratio as well as stable and reliable performance. It is well known that the manufacturing of aero-engines is an extremely complex engineering project, and the most central part is the blade, whose properties directly affects the safety and performance of aero-engines [1]. To achieve the maximum possible performance of the blades, the blades must be manufactured using a forming process, especially a hot forming process. This is because the required forming force of the hot forming process is significantly reduced, and the microstructure can be controlled so that the formability of the formed parts is increased [2]. A typical sequence for forming blades is shown in Fig. 1. The billet was preliminarily shaped by extrusion and heading, which are known as preforming. Then, the preform was forged to obtain the blade with flash. Multiple procedures are sequentially used in the typical process, and when the next procedure is executed, the billet must be heated and lubricant-coated again, which will significantly increase the instability and cost of the process. In addition, the hot forming of metals imparts considerable thermal and mechanical cyclic loads to the forming tools, which can particularly easily deteriorate the inner surface of the extrusion dies resulting in the loss of their service life. Moreover, the material properties of titanium alloy are characterized by lower thermal conductivity, which makes the deterioration more serious [3].

At present, local gathering upsetting and free forging can also be used as a preform procedure to manufacture aero-engine blades. Compared with the typical process, they consist of fewer production procedures. However, the major shortcoming is that the upsetting device is dedicated and high expensive which is not suitable for small batch production. Furthermore, the free forging has strong artificial dependencies and poor process stability and lower productivity. In consideration of the current imperfect forming process, cross-

✉ Junling Li
junlingli@ustb.edu.cn

[1] School of Mechanical Engineering, University of Science and Technology Beijing, No. 30 Xueyuan Road, Haidian District, Beijing 100083, China

[2] Beijing Institute of Aeronautical Materials, Beijing 100095, China

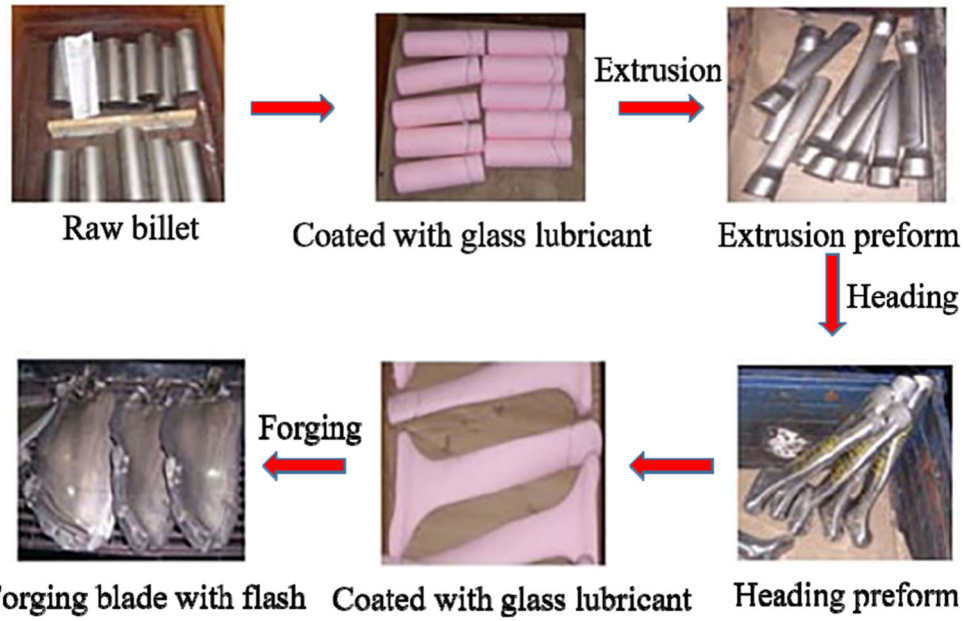

Fig. 1 A typical manufacturing process of turbine blades

wedge rolling (CWR) is innovatively applied to manufacture the aero-engine blade preform.

CWR is a near-net metal forming process in which the rotational parts are formed by two rolls with a wedge-shaped tool. Compared with the traditional process, the CWR process has advantages regarding saving materials and energy, lowering costs, increasing productivity, and improving the work environment which can meet the requirements of modern manufacturing [4]. In recent years, CWR has been applied not only to manufacture iron steel but also to alloys, and extensive studies have been conducted on CWR. Pater presented a method of modelling the process of CWR with upsetting, and this method allows determination of the rolling force, the contact surface between the material and tool and the rolling radius [5]. Afterward, Pater et al. presented the numerical analysis of the CWR process of ball pins, and the results showed that the application of the CWR method for the forming of ball pins is fully justified [6]. Li et al. presented a method for the prediction of the likelihood of void formation based on the definition of a non-dimensional deformation coefficient, and the three primary parameters can be optimized for tooling design [7]. Li et al. analyzed the fundamental CWR failure mechanisms through experimental and numerical research, and then discussed the industrial implementation of the CWR system and conducted several industrial examples [8]. Urankar et al. investigated the limits of forming hollow products with CWR by utilizing experiments and the explicit finite element method [9]. Bartnicki et al. also studied the aspects of stability in the CWR process of producing hollowed shafts. All of the literature above is aimed at forming steel parts with CWR [10]. With regard to alloys, Cakircali et al. applied the CWR process to Ti6Al4V(ELI) alloy to experimentally and numerically investigate the deformation and fracture [11]. Tofil et al. numerically and theoretically studied the CWR process for producing stepped shafts made of 6061 aluminum alloy, and this attempt was confirmed by CWR experiments [12]. Li et al. demonstrated a numerical and experimental investigation on the CWR of powder sintering TC4 alloy, and the results showed that using the CWR process to produce powder sintering TC4 alloy is feasible, and the requirements of plastic forming, densification, and mechanical performance can be completely satisfied [13]. Mirahmadi et al. investigated the effect of CWR tool parameters on the formability of Nimonic® 80A and Nimonic® 115 wrought superalloy using the Cockcroft-Latham model; the results showed that the low wedge and stretching angles are beneficial to manufacturing sound parts [14].

At present, some researchers are attempting to apply the CWR process to manufacturing shaft preform, such as hollow valves [15, 16], as well as non-shaft preforms, such as crankshafts, hip implants [17], and blades [18]. Ji et al. developed a new method for manufacturing hollow valves via a CWR and forging process, and a numerical model of CWR-forging using the finite element method (FEM) was built to estimate the practicability of the compound processes, and the verified by laboratory experiments [15, 19]. Meyer et al. described the development of a four stage process chain for manufacturing a crankshaft with a pin and flange [20]. The first preforming step is CWR, providing the essential volume reallocation for pin bearings and crank arms. To reduce the production cost and save the valuable titanium alloy, an existing forging sequence with CWR as a preforming operation for manufacturing hip implants was investigated by Behrens et al. [17]. The results showed that the newly developed composite process significantly reduced the flash rate from 69 to 32%. Li et al. presented an investigation on the effects of CWR parameters

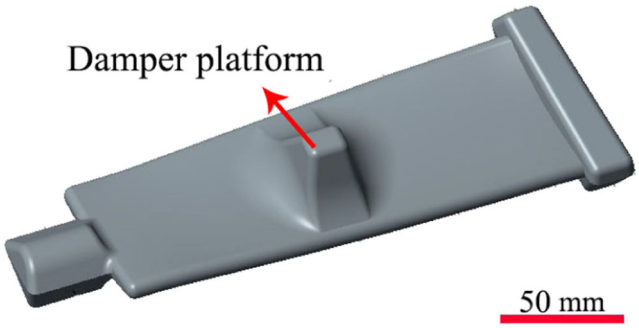

Fig. 2 Compressor blade with a tenon and damper platform

on the formability of Ti-6Al-4 V alloy blade preforms, and safe process parameters were obtained. However, the subsequent forging process was not involved [18].

In the present study, a new process chain combining CWR and isothermal forging has been proposed to manufacture titanium alloy aero-engine blades. Firstly, a proper preform of the target blade was designed under the guidance of the equal area criterion. Then, the new process chain for manufacturing the blade was numerically modelled, and the fundamental deformation mechanism was analyzed. Finally, the corresponding experiments were conducted to verify the new sequence.

2 Target analysis and preform design

Figure 2 shows the turbine blade made of titanium alloy. This kind of blade typically has a long body and large twisting angles, and the total length and height of the blade is approximately 200 mm and 50 mm. Moreover, there is a damper platform in the center of the blade body and a large difference in geometric size between the tenon, damper platform, and blade tip. All

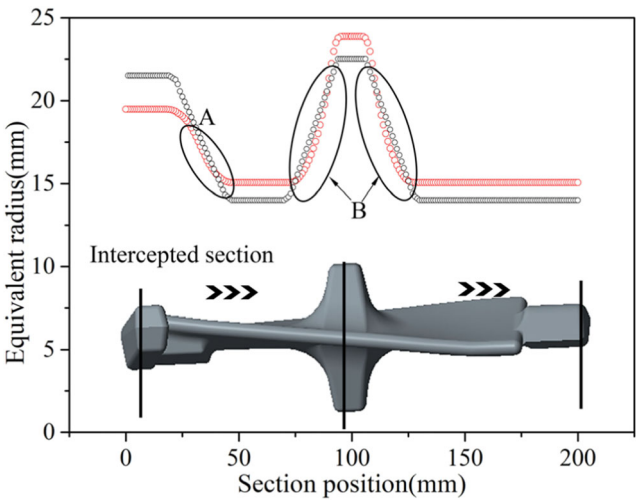

Fig. 3 The distribution of equivalent radii before and after modification

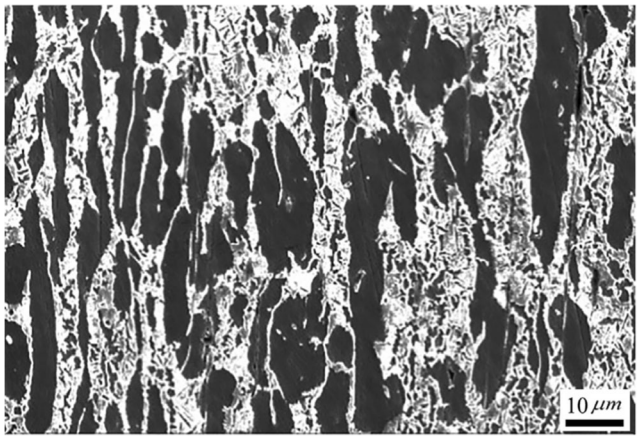

Fig. 4 The initial microstructure of the studied TC6 alloy

of these features make it more difficult to preform the table by the CWR process.

Preforming is a very important stage to realize the volume redistribution of the billet and the shape preforming of the final product. The preform design can be done through the backward deformation according to style of the final blade. However, a forward consideration related to the difficulty of the preform stage is also required. Therefore, a round bar was used to attempt to accomplish the volume redistribution.

To obtain a satisfactory volume distribution of the preform, it is necessary to develop an appropriate criterion. It is well known that isothermal forging is a near-net-shape bulk

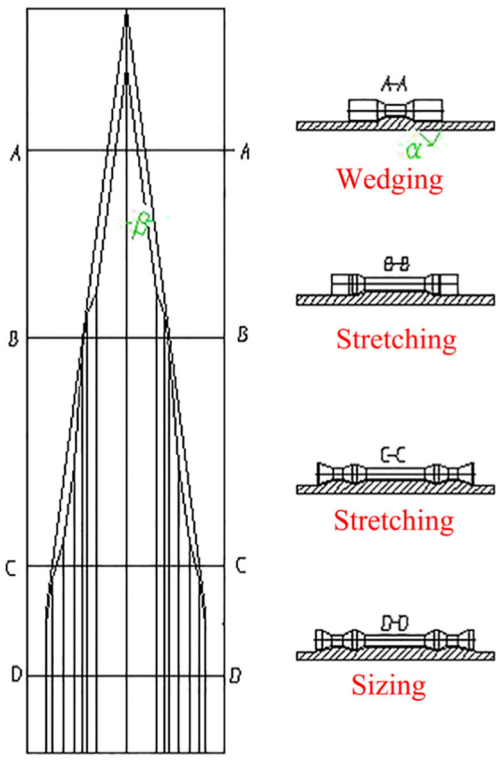

Fig. 5 Flattened diagram of the CWR tool for pair rolling

Table 1 Main thermal parameters for the CWR simulation

Parameter	Value
Heat transfer coefficient (N/s/mm/°C)	11
Convection coefficient (N/s/mm/°C)	0.02
Emissivity (N/s/mm/°C)	0.7
Initial billet temperature (°C)	890
Tool temperature (°C)	20
Environment temperature (°C)	20
Mechanical to heat	0.9
Rolling speed (r/min)	8

forming process, so equal volumes are expected between the preform and the final blade. Therefore, the equal area criterion is ideally suited for guiding the preform design. First, sections of the final part shown in Fig. 3 with an interval of 1 mm along the axis direction were intercepted to measure its active area, S_{ar} (mm^2). Second, the equivalent radius, R_{eq} (mm), of each section was calculated according to the measured area. The equivalent radii of the initial preform were plotted in red symbols as shown in Fig. 3. The equivalent radii in districts A and B were changed nonlinearly, which is difficult to achieve using the CWR process. Thus, the equivalent radii need to be appropriately modified.

In consideration of the significance and difficulty of the preform design, especially for the studied parts with complex shapes, it is very important to seek a balance between the CWR and isothermal forging stages. On the one hand, a desirable preform should resemble the finale part to ensure a smooth, streamlined surface, to reduce the forging force, and to obtain sufficient flash-filling. On the other hand, the CWR process is very adept at forming stepped shaft parts with linear connections between different steps. Moreover, improving the deformation uniformity can be conducive to elevating the forming accuracy and simplicity. With the help of the numerical simulation of the forging process and after establishing a series of dimensional coordinates from

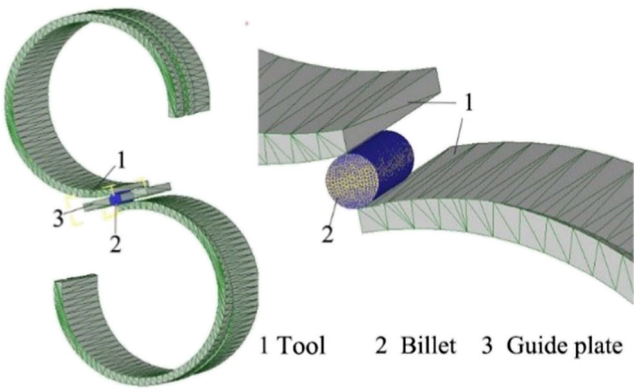

Fig. 6 The geometry model for the CWR process

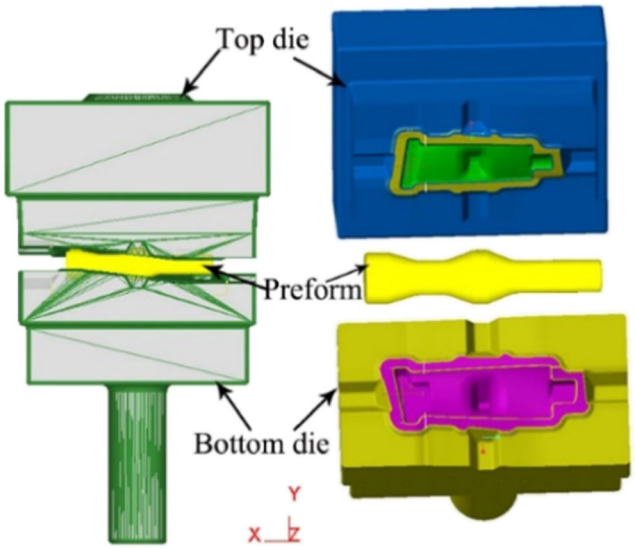

Fig. 7 3D geometric model for preform forging

the CWR experiment experience, the final modified equivalent radius was determined, as shown by the black symbol in Fig. 3. The nonlinearity of the equivalent radius was simplified to a linear change, which facilitates the formability during the CWR process.

3 Numerical modelling of the new sequence

3.1 Material characteristic

The TC6 (Ti-6Al-1.5Cr-2.5Mo-0.5Fe-0.3Si) titanium alloy can preserve its material characteristics under high working temperatures up to 450 °C. In addition, the titanium alloy has high specific strength, which makes it an ideal material for aero-engine blades. It has been reported that the TC6 alloy is sensitive to deformation parameters, and the Arrhenius equation is widely applied to describe the deformation behavior at high temperature. In the present study, the material used was a TC6 bar material provided by Baoti Co., Ltd, and the initial microstructure is shown in Fig. 4. It mainly consists of the long-strip alpha phase and a couple of equiaxed alpha phases dispersed throughout the matrix. The hot compression was conducted on the Gleeble-1500D thermo-simulation machine,

Fig. 8 The manufactured die of the H630 machine

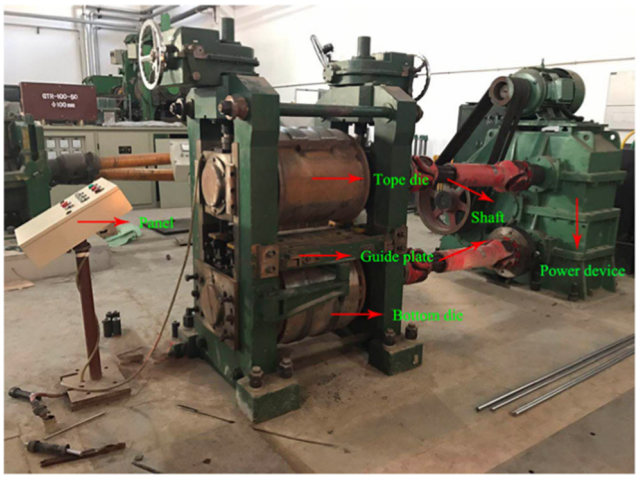

Fig. 9 H630 CWR machine used in the experiment

and based on the beta transus temperature of 985 °C, the deformation temperature, T (°C), and strain rate, $\overline{\varepsilon}$ (s^{-1}), were set to 850, 910, and 970 °C and 0.1, 1.0, 10 s^{-1}, respectively [21]. The Arrhenius equation was used to elaborate the relationship between deformation parameters and flow stress as follows.

$$\varepsilon = A[\sinh(\alpha\sigma)^n]\exp\left(\frac{-Q}{RT}\right) \quad (1)$$

where Q (J mol^{-1}) is the activation energy of the titanium alloy, R is the universal gas constant of 8.3145 J mol^{-1} K^{-1}, while A, α, and n are the constants.

All the pending constants were determined by the flow stress-strain data at a strain (ε) of 0.5 through a series of mathematical calculations, as shown in the work of Peng et al. [22]. Finally, the constitutive equation was implemented into the Deform-3D software material library to ensure the accuracy and reliability of the FE simulation results.

$$\varepsilon = e^{54062}[\sinh(0.01778\sigma))^{3.399}]\exp\left(\frac{-563839.96}{RT}\right) \quad (2)$$

3.2 Numerical modelling of the cross-wedge rolling process

3.2.1 Design of the tools

Symmetric rolling is one of the basic principles of the design of the CWR tool; however, the optimized preform is not equipped with symmetrical features. Generally, four basic methods can be serviceable: (1) pairs rolling, (2) section symmetrical rolling, (3) symmetric force rolling, and (4) pre-rolling. By thoroughly considering its features and requirements, the method of pairs rolling was applied in the tool design, which can simultaneously meet the challenges of doubling production and saving materials, but the rolled parts should be cut off artificially. Figure 5 presents the flattened diagram of the CWR tool for pair rolling. First, deformation occurs in the symmetrical section of the billet once the first wedge is applied (A-A), and then the billet starts to stretch when compressed by the upper and lower tools (B-B) until it meets the second wedge (C-C), and different sections are deformed. Ultimately, the billet continuously rolls to be sized (D-D). During the CWR process, problems, such as plastic bending deformation, spiral mark, necking, and fracture, are likely to happen. Hence, reasonable tool parameters need be chosen to improve the CWR formability. Based on forming experience with the CWR process, and reducing the tool length to meet the demand of the H630 rolling mill, the forming angle α and stretching angle β are 25° and 7.5°, respectively.

3.2.2 The FE model of the CWR process

A 3D rigid-plastic FE model was developed based on the following assumptions. (1) Only the billet was considered to be a plastic body, all of the tools and guide plates were regarded as rigid bodies due to the negligible deformation. (2) Due to the symmetry of the FE model, a symmetrical boundary was applied to the symmetrical section to reduce the total computing time. (3) The shear friction model was applied to describe the friction of the contact surface between the tools and billet, and the friction coefficient is set to 2 in order to promote the rotation to make the rolls smoothly wedged. (4) The heat convection between the billet and the environment, as well as the heat transfer between the billet and tools are summarized in Table 1 along with other thermal parameters. (5) All the CWR experiments were carried out on the H630 CWR mill, so the rotational speed of the roller maintains a constant speed of 8 r/min. Figure 6 presents the geometric model of the CWR process, which is composed of two tools, two guide plates and a billet.

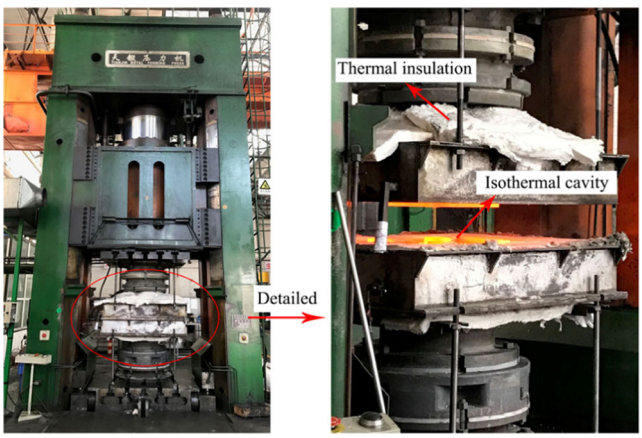

Fig. 10 The isothermal die forging mill used in the experiment

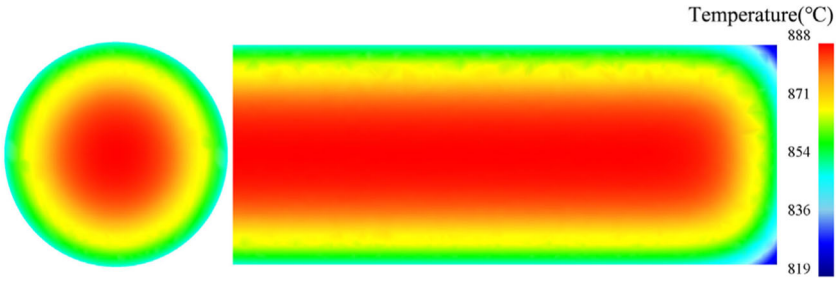

Fig. 11 Temperature distribution on the cross- and longitudinal sections at the end of transfer process

It is well known that titanium alloy is very sensitive to the deformation temperature. Therefore, the transfer process from the resistance-heated furnace to the CWR mill was considered. This process was simulated by a static heat transfer model, and only the heat convection between the billet and the surrounding air at room temperature was defined; this process lasted for 10 s according to the CWR experiment.

3.3 Numerical modelling of the isothermal forging process

The forging procedure is the final procedure for forming the blade. To examine the forming performance of the designed preform during the isothermal forging process, a 3D geometric model of the preform forging, which consists of a top die, preform, and bottom die, was built, as shown in Fig. 7. The dies were regarded as rigid bodies due to their negligible plastic deformation. In contrast, the preform was a plastic body, and meshed by 80,000 grid with a minimum length less than 1 mm. The friction between the dies and the workpiece were modelled by the shear model, and the friction factor, μ, was 0.3 due to the glass lubrication in the practice experiments. In addition, the applicable temperature of the TC6 alloy preform during the isothermal die forging is between 915 °C and 935 °C, and the temperature difference is within 5 °C between the preform and the dies. In this paper, the forging temperature was set to 925 °C. In addition, there is very little heat transfer between the surface of the preform and the dies, so the heat transfer coefficient is zero. Another important parameter is the die speed. In isothermal die forging, the die moved down at the speed of 0.1 mm/s along the *Y*-axis.

4 Experimental work with the new sequence

The corresponding experimental work with the new sequence was carried out to verify the reliably of the finite element simulation results. It is expected that the compressed blade can be successfully manufactured by using this new sequence. The CWR dies were manufactured based on the design diagram, as shown in Fig. 8. Then, the dies were installed and fixed on the H630 machine, as shown in Fig. 9.

The forging experiments were carried out in an isothermal die forging mill with a maximum forging force of 20000 KN. The dies are made of N3 alloy developed by the Beijing Institute of Aeronautical Materials. The die cavity was heated to the preset temperature, and covered by thermally-insulating protective asbestos (Fig. 10).

5 Results and discussion

5.1 Transfer process

Figure 11 presents the temperature field distribution of the cross- and longitudinal sections at the end of the transfer process. Not surprisingly, the temperatures along the radial direction progressively decrease from the billet center to the surface. In the tail end of the billet, the temperature falls sharply to 819 °C, which reaches a maximum drop of 7.8%. However, in other locations, the temperature remains in the range of 850~890 °C. For the quantitative analysis, the change curves of the temperature of with five tracepoints were plotted, as shown in Fig. 12. There is a drop within 10 °C in the temperature of the tracepoints P11, P12, and P13. However, the temperature reduction of tracepoint P15 is up to 40 °C after the transfer process.

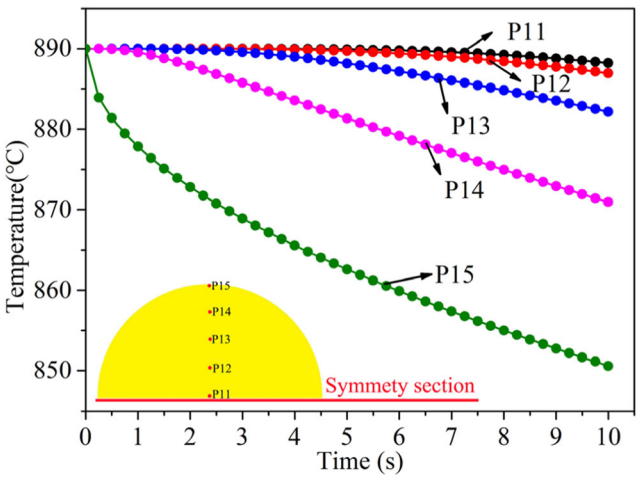

Fig. 12 Change curves of the temperature of five tracepoints during the transfer process

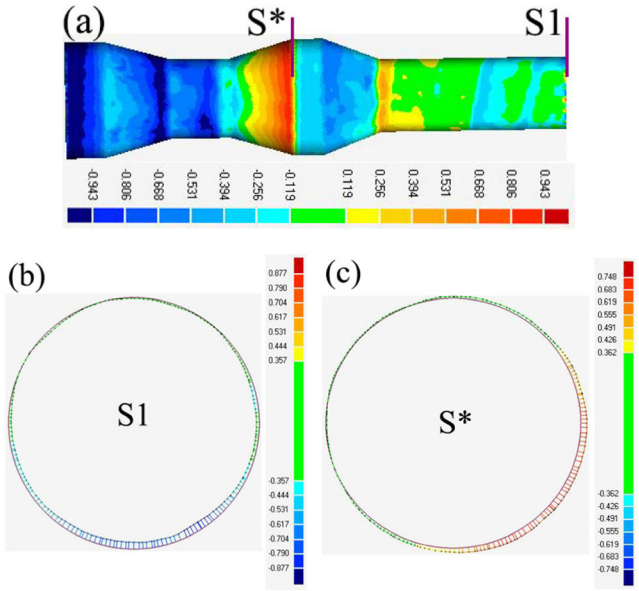

Fig. 13 Comparison of the cross-wedge rolling part and simulated results

Thus, the temperature reduction and distance from the center do not show a linear relationship.

5.2 Cross-wedge rolling process

5.2.1 Verification of the CWR FE model

A comparison of the cross-wedge rolling part and the simulated result is illustrated in Fig. 13. For a more accurate comparison, the geometric data of the CWR part was extracted by a 3D scanner with high precision, and then the geometrical dimensions of the CWR part were compared with the simulated result by using Geomagic Quality software. As Fig. 13a shows, the maximum and minimum radial errors were 0.943 mm and − 0.943 mm, respectively. This indicates that the FE model is reliable. In the wedge position, as shown in Fig. 13b, the radial errors were negative, which means that a very slight necking occurred. In contrast, it is more prone to stockpile in section S*. Therefore, in the actual CWR experiment, it is necessary to properly polish the wedge tip and carefully check the material flow near section S*.

5.2.2 Axial displacement analysis

Although the CWR process has been proven to be one mature and economical application technology for the formation of steel parts, the formation process of titanium alloy parts is considerably more difficult than that of steel parts. It is well known that titanium alloy has high viscosity and irregular liquid characteristics, so movement in the axial direction during the CWR process of titanium alloy parts is a serious issue. Figure 14 shows the distribution of the six tracepoints with evenly spaced increments of 20 mm on a longitudinal section before and after the CWR process. It is obvious that the relative displacement of P21 is the largest due to the axial extension in the stretching area. Moreover, the relative displacement of P41 is the smallest due to the restriction of the second wedge; it is also the reason for the material stockpile problem in section S*. Quantitative analysis results are shown in Fig. 15, indicating that the axial displacements of P21, P31, and P41 initially increase linearly and then remain steady during the whole process. Moreover, another increase in the axial displacements of P51 and P61 appears due to the second wedging. However, there is no fluctuation in any of the axial displacement curves, which indicates that the deformed material in the center experiences a smooth flow during the whole CWR process.

In addition to the movement of the center materials, it is also necessary to investigate the axial displacement in the same section. Previous studies have suggested that concavity at the end of the steel parts was formed during the CWR process, and the large concavity not only results in material loss but also causes central damage [23]. Figure 16 shows the axial displacement change curves of the tracepoints on two cross-sections during the CWR process. It is obvious that the axial displacement of the five tracepoints on section S2 is simultaneously increasing until section S2 is rolled as shown in Fig. 16a. After the instantaneous deformation, the axial flow of surface point P25 slightly lags behind the inner materials, and the final differences between the surface and center tracepoints is 2.23 mm, which is small enough to be ignored. The same thing is true with section S6, as shown in Fig. 16b. Unlike steel parts, there is no large concavity at the end of the titanium alloy parts, which could be due to the higher

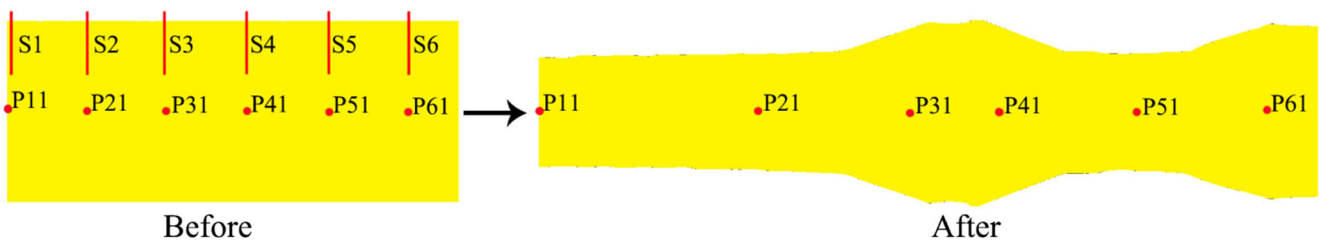

Fig. 14 Distribution of the tracepoints on longitudinal section before and after the CWR process

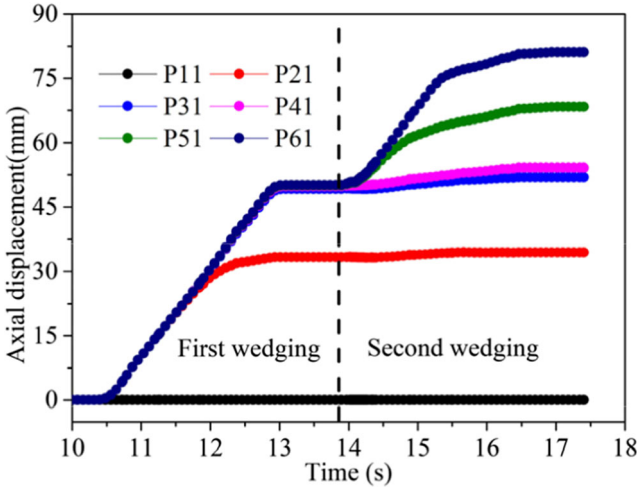

Fig. 15 Change curves of the axial displacement of the tracepoints on longitudinal section during the CWR process

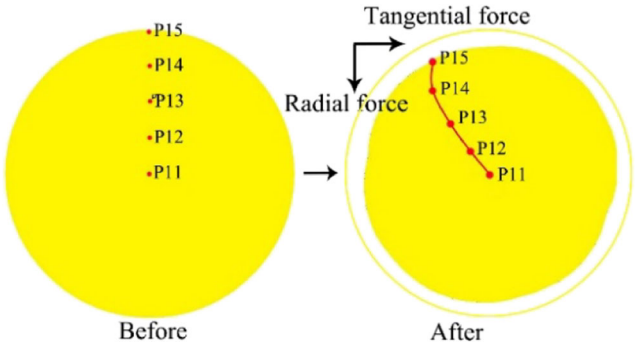

Fig. 17 Distribution of the tracepoints on cross-section S1 before and after the CWR process

viscosity. To be more specific, it may also be related to the difference of the crystal structures, which demands further verification.

5.2.3 Temperature analysis

Another important feature concerning titanium alloy is the lower thermal conductivity, which makes it more difficult to maintain a balanced temperature distribution than for steel parts. In the CWR process, the billet experiences three different heat transfer mechanisms leading to the thermal dissipation and temperature drop. However, the billet also undergoes large plastic deformation resulting in the thermal conversion from the deformation energy. Therefore, the stress-strain state will significantly affect the temperature distribution. The distribution of the tracepoints on the symmetrical section S1 before and after the CWR process is shown in Fig. 17. The tracepoints fall in a straight line along the radius prior to the deformation, and the straight line is obviously distorted after the CWR process, which means that the rolled part is not only radially compressed and axially expanded but also tangentially moved due to the friction. This is the result of the collaborative effect of radial, axial, and tangential forces. The collaborative effect of different forces varies even in the same section, which will directly impact the temperature distribution. Therefore, the effective strain and stress and the corresponding temperature distribution are analyzed.

Figure 18 a shows the effective strain on the symmetric section S1. All the effective strain curves sharply increase and then become steady during the first wedging. As the rolled part sustains the second wedging, the effective stain curves of the tracepoints P13, P14, and P15 exhibit a similar steady increase. However, the tracepoints P11 and P12 located near the center are unresponsive. For the effective stress, all the curves have similar varying tendencies, and peaks appear at moment of deformation. However, the peak stress of tracepoint P15 is up to 250 MPa, which is much larger than those of the other tracepoints, and tracepoint P15 is located on the surface of the rolled part. Therefore, this peak stress is a result of the work-hardening effect, when the parts are directly in contact with the cold dies, the surface materials of the rolled part will be momentary cold-hardened, also known as chilling effect, and the corresponding temperature drop is shown in Fig. 18c. Meanwhile, the deformation-heat and friction-heat will counterbalance the heat loss and

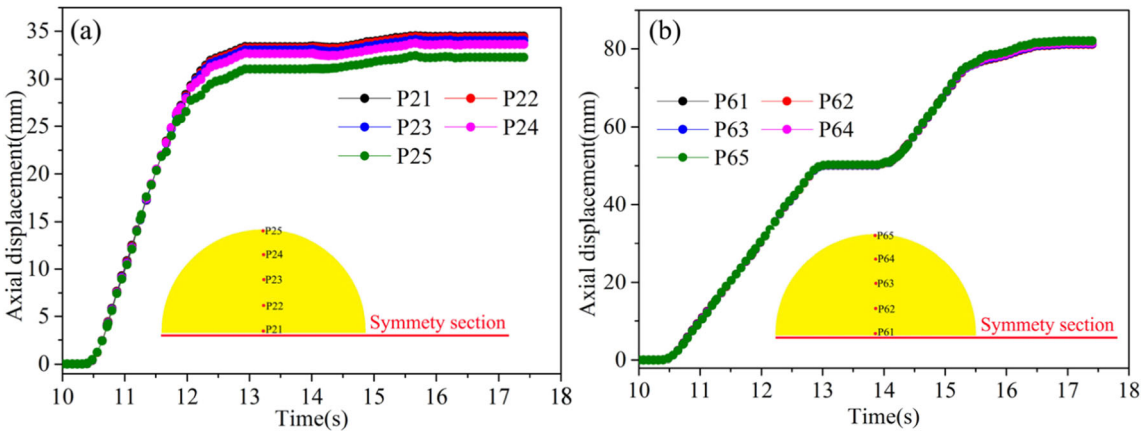

Fig. 16 Change curves of the axial displacement of the tracepoints on cross-sections during the CWR process

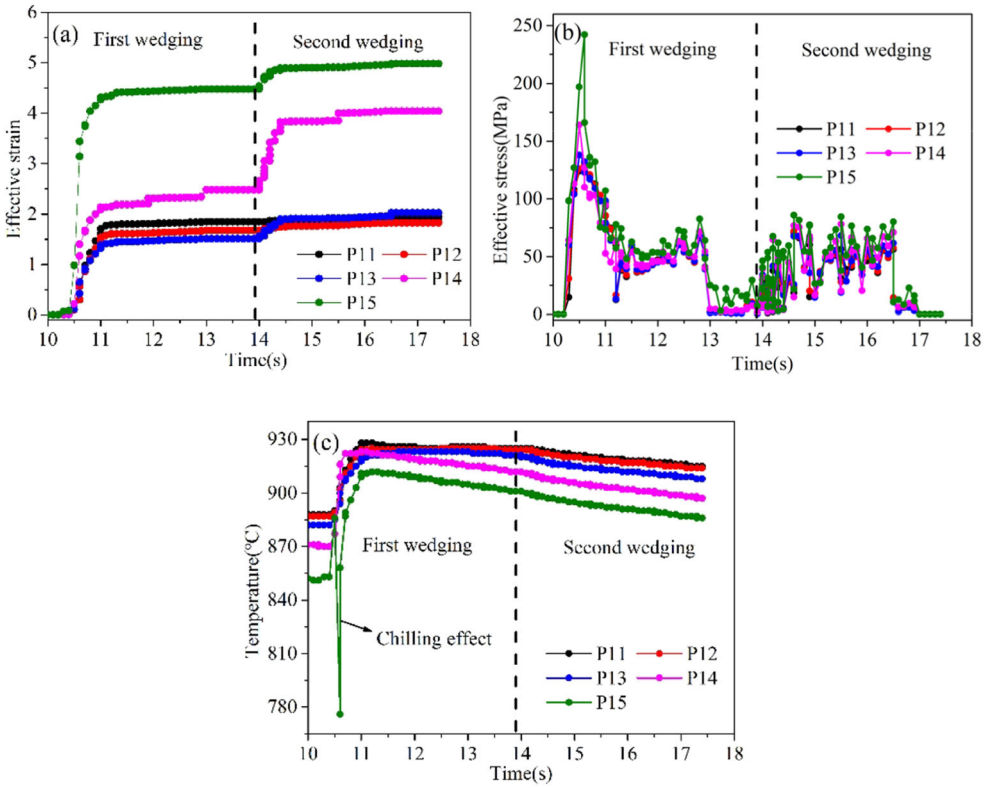

Fig. 18 Change curves of the effective strain and stress along with temperature: **a** effective strain, **b** effective stress, and **c** temperature

increase the transient temperature. Finally, the temperature difference between the tracepoints P15 and P11 is approximately 25 °C. However, if the chilling effect becomes worse or heat loss can not be efficient replenished, it will be difficult for deformation to continue. This will also increase the temperature inhomogeneity and adversely affect the mechanical properties of the rolled part. To avoid the negative impact of the chilling effect, sometimes it is necessary to preheat the dies.

5.2.4 Microstructure analysis

The microstructure of the rolled part is a direct result of the deformation process and determines the mechanical

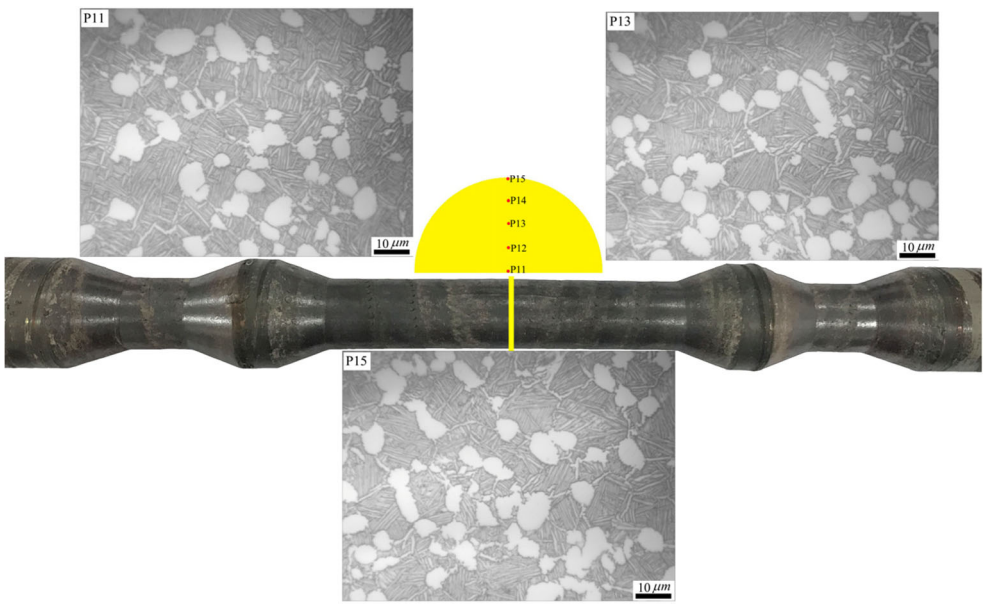

Fig. 19 Microstructure of the rolled part after the CWR process

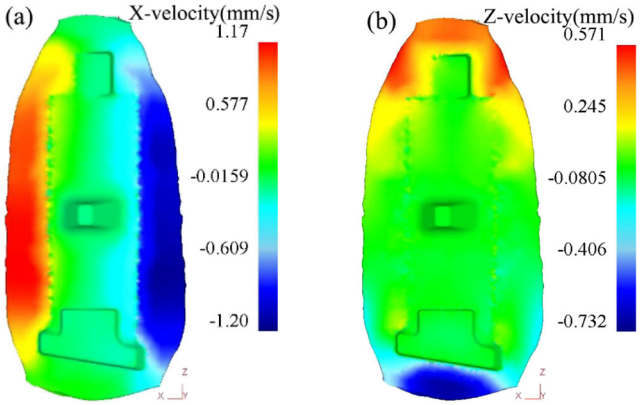

Fig. 20 Velocity distribution of the preform during isothermal forging: **a** *X*-velocity and **b** *Z*-velocity

properties. The microstructure of the rolled part after the CWR process is presented in Fig. 19. The microstructure consists of an equiaxed primary alpha phase and a lamellar secondary alpha phase with a regular distribution as well as a few intergranular beta phase regions. Moreover, the microstructure of three different tracepoints shows consistency which means there are no large temperature differences in the rolled part. Compared with the initial microstructure as shown in Fig. 4, the long-strip alpha phase disappeared, and more of the equiaxed alpha phase appeared instead. This is because the large plastic deformation induced the globularization of the long-strip alpha phase, which means that the long-strip alpha phase was bent, fractured, and equiaxed during the CWR process. The existing research shows that the bimodal structure possesses higher plasticity and fatigue strength, and by controlling the proportion of the equiaxed and lamellar alpha phase, the microstructure can achieve a better overall performance. Therefore, it is necessary to investigate the effect of the process parameters on the microstructure evolution in the further study. In this paper, the microstructure of the rolled part demonstrates that there are no large temperature differences and that the microstructure distribution is uniform. Importantly, the CWR process enhances the mechanical performance of the titanium alloy parts.

5.3 Isothermal forging process

5.3.1 Velocity analysis

Figure 20 shows the flowing velocity of the preform along the *X*-axis and *Z*-axis during isothermal forging. It is obvious that the maximum velocities of the *X*-axis in the positive and negative directions are 1.17 mm/s and − 1.20 mm/s, respectively, which are nearly equal in magnitude. The *X*-velocity is symmetrically distributed with the center line of the blade, which suggests that the deformation along the *X*-axis is uniform. The *Z*-velocity achieves its extreme values at the upper and lower ends, and the *Z*-velocity values in the blade are almost uniform but slightly less than those of the *X*-velocity. The velocity distribution suggests that the material flow of the preform is mainly horizontally and vertically expanded with the *Y*-axis compressed.

5.3.2 Strain and stress analysis

The strain field of the blade with flash during isothermal forging is shown in Fig. 21. The *X*-axis and *Z*-axis strains of the sharp corner of the tenon and the blade tip in contact with the dies' cavities are almost zero, but the *Y*-axis strain is at its maximum value. This is due to the restriction of the cavities; the deformed material could only flow along the *Y*-axis. Judging from the entire blade with flash, the *X*-axis strain tends towards a symmetrical distribution, and the *Z*-axis strain is equally distributed except for the damper platform.

5.3.3 Microstructure analysis

The maximum principal stress of the preform during isotheral forging is shown in Fig. 22. On the edge of the flash, the maximum principal stress is up to 86 MPa, which

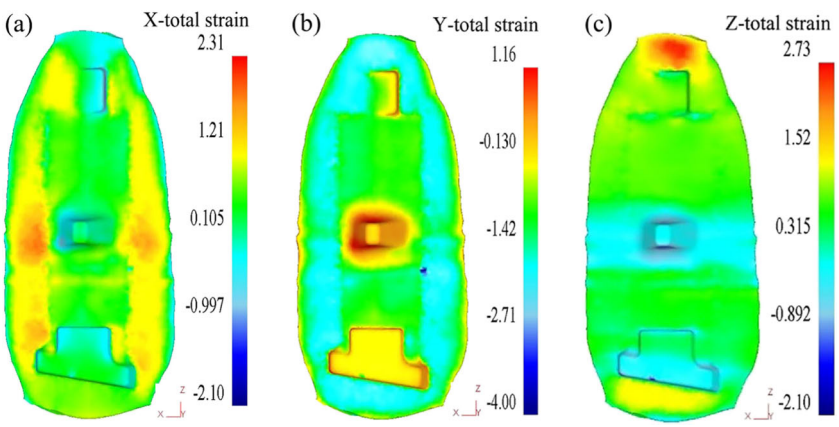

Fig. 21 Strain distribution of the preform during isothermal forging: **a** *X*-total strain, **b** *Y*-total strain, and **c** *Z*-total strain

indicates that areas are subject to tension. When the tensile stress exceeds the limit, cracking and other forming defects will occur. However, over the entire body of the blade, the maximum principal stress is significantly negative, and leads to better deformation of the microstructure and mechanical properties.

The TC6 alloy blade with and without flash after isothermal forging is shown in Fig. 23. There are no obvious folds, unfilled areas, or other forming defects, and the flash is symmetrically distributed around the blade. The right graph shows the blade with the flash being water-jet cut, illustrating that the damper platform, the blade tip, and the tenon are fully filled. Just as important, we examined the microstructure of the blade after isothermal forging, as shown in Fig. 24. The deformed microstructure also consists of the equiaxed primary alpha phase and a few intergranular beta phase regions. The difference is that the volume fraction of the primary alpha phase obviously increased, and the lamellar alpha phase forms short rod that are distributed more randomly. This is more beneficial to improving the combination performance, especially the toughness.

6 Conclusion

In this paper, a new process chain for forming the compressor blades with damper platform by CWR and isothermal forging was proposed, and it was systematic analyzed with a combination of FE numerical simulation and experimental verification. The following conclusions were drawn:

1. For a turbine blade made of titanium alloy and with a damper platform, a new process chain combining CWR and isothermal forging was proposed, and a reasonable and appropriate preform was designed giving consideration to both the forming difficulty of the CWR process and the formability of the isothermal forging process. The new process chain can significantly increase productivity, lower product costs, and improve the combination performance.
2. A FE model including the transfer, CWR, and isothermal process was developed and used to investigate the whole new sequence. After the transfer process, the temperatures progressively decrease from the center to the surface, and the temperature reduction and distance from the center is not a linear relationship.
3. There is no fluctuation in all the axial displacement curves of the tracepoints in the center along the axial direction, indicating a smooth flow. On the same cross-section, the axial flow of the surface point slightly lags behind the inner materials, but the final difference is small enough to be ignored. All these factors suggest that there is no large concavity at the tail end of the titanium alloy parts due to the higher viscosity.
4. The materials near the surface sustain larger deformation, the deformation-heat and friction-heat counterbalance the heat loss due to the chilling effect, and the final

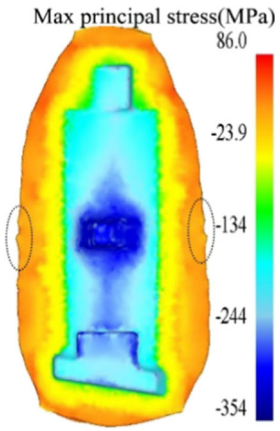

Fig. 22 Stress distribution of the preform in the isothermal forging process

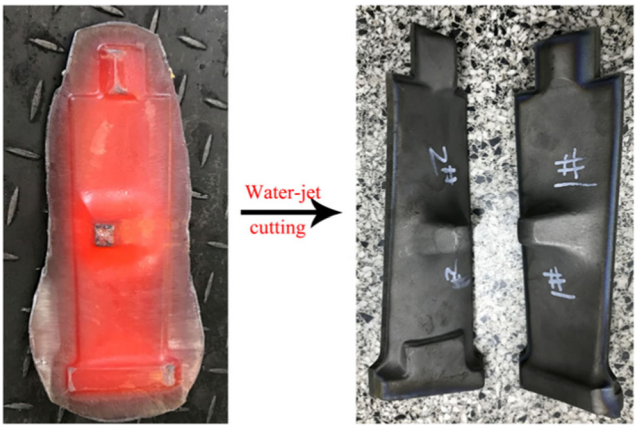

Fig. 23 TC6 alloy blade with and without flash after isothermal forging process

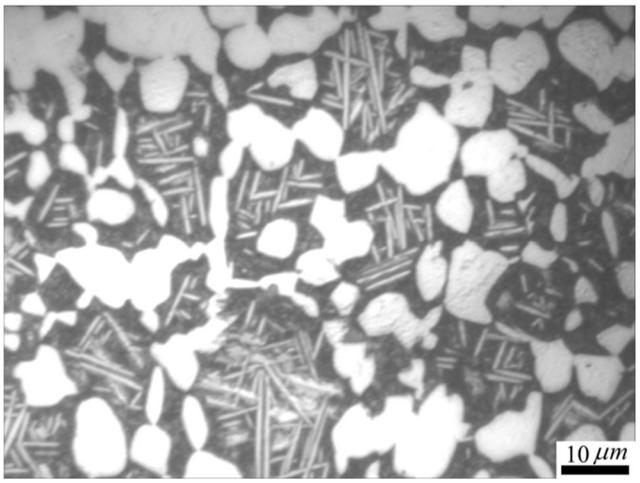

Fig. 24 Microstructure of the blade after isothermal forging process

temperature difference between the center and surface is approximately 25 °C. The microstructure with a uniform distribution also demonstrates no large temperature difference. Moreover, the microstructure is significantly improved by accelerating the globularization of the long-strip alpha phase.

5. The flash is symmetrically distributed around the TC6 alloy blade, and no obvious forming defects occur. The damper platform, blade tip, and tenon are fully filled after the isothermal forging process. Moreover, the volume fraction of the primary alpha phase obviously increased, and the lamellar alpha phase forms short rods that are distributed more randomly, which is more beneficial to improving the combination performance, especially the toughness.

Funding information This work is supported by the Fundamental Research Funds for the Central Universities (grant no. FRF-TP-19-043A1).

References

1. Liu YL, Yang H, Zhan M, Fu ZX (2002) A study of the influence of the friction conditions on the forging process of a blade with a tenon. J Mater Process Technol 123:42–46
2. Huang SH, Zong YY, Shan DB (2013) Application of thermohydrogen processing to Ti6Al4V alloy blade isothermal forging. Mater Sci Eng A 561:17–25
3. Painter B, Shivpuri R, Altan T (1996) Prediction of die wear during hot-extrusion of engine valves. J Mater Process Technol 59:132–143
4. Yang CP, Zheng ZH, Hu ZH (2018) Simulation and experimental study on the concavity of workpiece formed by cross wedge rolling without stub bar. Int J Adv Manuf Technol 95:707–717
5. Pater Z (1998) A study of cross wedge rolling process. J Mater Process Technol 80-81:70–375
6. Pater Z, Bartnicki J, Samołyk G (2005) Numerical modelling of cross-wedge rolling process of ball pin. J Mater Process Technol 164-165:1235–1240
7. Li Q, Lovell M, Slaughter W, Tagavi K (2002) Investigation of the morphology of internal defects in cross wedge rolling. J Mater Process Technol 125:248–257
8. Li Q, Lovell M (2008) Cross wedge rolling failure mechanisms and industrial application. Int J Adv Manuf Technol 37:265–278
9. Urankar S, Lovell M, Morrow C, Li Q, Kawada K (2006) Establishment of failure conditions for the cross-wedge rolling of hollow shafts. J Mater Process Technol 177:545–549
10. Bartnicki J, Pater Z (2004) The aspects of stability in cross-wedge rolling processes of hollowed shafts. J Mater Process Technol 155-156:1867–1873
11. Cakircali M, Kilicaslan C, Guden M, Kiranli E, Shchukin YV, Petronko VV (2013) Cross wedge rolling of a Ti6Al4V (ELI) alloy: the experimental studies and the finite element simulation of the. Int J Adv Manuf Technol 65:1273–1287
12. Tofil A, Tomczak J, Bulzak T (2015) Numerical and experimental study on producing aluminum alloy 6061 shafts by cross wedge rolling using a universal rolling mill. Arch Metall Mater 60:801–807
13. Li JL, Wang BY, Ji HC, Zhou J, Huang X (2018) Numerical and experimental investigation on the cross-wedge rolling of powder sintering TC4 alloy. Int J Adv Manuf Technol 94:2149–2162
14. Javid SM, Mohsen H, Shahabeddin A (2014) Investigating the effects of cross wedge rolling tool parameters on formability of Nimonic® 80A and Nimonic® 115 superalloys. Int J Adv Manuf Technol 74:995–1004
15. Ji HC, Liu JP, Wang BY, Zhang ZR, Zhang T, Hu ZH (2015) Numerical analysis and experiment on cross wedge rolling and forging for engine valves. J Mater Process Technol 221:233–242
16. Pater Z, Gontarz A, Tomczak J (2015) Producing hollow drive shafts by rotary compression. Arch Civ Mech Eng 15:917–924
17. Behrens BA, Stonis M, Blohm T (2016) Investigating the effects of cross wedge rolling preforming operation and die forging with flash brakes on forging titanium hip implants. Int J Mater Form 11:67–76
18. Li JL, Wang BY, Ji HC, Huang X, Tang XF, Ma WP (2017) Effects of the cross-wedge rolling parameters on the formability of Ti-6Al-4 V alloy. Int J Adv Manuf Technol 92:2217–2229
19. Ji HC, Liu JP, Wang BY, Fu XB, Xiao WC, Hu ZH (2017) A new method for manufacturing hollow valves via cross wedge rolling and forging: Numerical analysis and experiment validation. J Mater Process Technol 240:1–11
20. Meyer M, Stonis M, Behrens B (2015) Cross wedge rolling and bi-directional forging of preforms for crankshafts. Prod Eng 9:61–71
21. Li JL, Wang BY, Huang H, Fang S, Chen P, Shen JX (2018) Unified modelling of the flow behavior and softening mechanism of a TC6 titanium alloy during hot deformation. J Alloys Compd 748:1031–1043
22. Peng X, Guo H, Shi Z, Qin C, Zhao Z (2013) Constitutive equations for high temperature flow stress of TC4-DT alloy incorporating strain, strain rate and temperature. Mater Des 50:198–206
23. Yang CP, Dong HB, Hu ZH (2018) Micro-mechanism of central damage formation during cross wedge rolling. J Mater Process Technol 252:322–332

Publisher's note Springer Nature remains neutral with regard to jurisdictional claims in published maps and institutional affiliations.